Design and Wind Tunnel Testing of a Thick, Multi-Element High-Lift Airfoil

Zahle, Frederik; Gaunaa, Mac; Sørensen, Niels N.; Bak, Christian

Published in:
Proceedings of EWEA 2012 - European Wind Energy Conference & Exhibition

Publication date:
2012

Document Version
Publisher's PDF, also known as Version of record

Design and Wind Tunnel Testing of a Thick, Multi-Element High-Lift Airfoil

Frederik Zahle, Mac Gaunaa, Niels N. Sørensen, Christian Bak
Wind Energy Department, DTU, DK-4000 Roskilde, Denmark
frza@dtu.dk

Abstract

In this work a 2D CFD solver has been used to optimize the shape of a leading edge slat with a chord length of 30% of the main airfoil which was 40% thick. The airfoil configuration was subsequently tested in a wind tunnel and compared to numerical predictions. The multi-element airfoil was predicted to achieve a C_{l-max} of 3.1 based on the main airfoil chord length, which was confirmed in the wind tunnel campaign. Using wake rake traversal and wool tuft flow visualization wall interference effects were investigated, which were found to be a source of considerable uncertainty when measuring on thick airfoils.

1 Introduction

One of the main challenges to the continuous up-scaling of wind turbines is to maintain low weight while achieving the necessary stiffness of the blade. An important parameter to achieve high stiffness is the relative thickness of the airfoils on the blade. Modern blade designs therefore move towards using thicker airfoils to maintain high stiffness while minimizing the weight. However, an increase in relative thickness of the blade poses considerable aerodynamic challenges, since thick airfoils are generally less efficient than thinner ones. Few such airfoils exist, and there is thus a need to design and validate dedicated thick airfoils for the next generation of large MW wind turbines. It is well-known, however, that both simulations and wind tunnel measurements on thick airfoils are associated with considerable challenges, which need to be addressed to increase reliability of the airfoil data used to design wind turbines.

In traditional rotor designs not much attention has been paid to the design of the innermost 20% of the blade. Recent studies have, however, pointed out that a higher loading towards the root of the rotor can yield higher energy production [3]. Rotor designs have been investigated which achieve this using very large chord lengths in the root area [2], where it was shown that considerable gains in energy production can indeed be achieved. Large blade root chords are, however, for a number of reasons not a very desirable design choice. This is why recent studies have turned to multiple element airfoils [1, 10], which by Gaunaa and Sørensen [1] were shown to be able to achieve lift coefficients above 2.5 using a main airfoil with a thickness of 36% fitted a slat with a chord length of 30% of the main airfoil chord. Multiple element airfoils are still a quite unexplored field within the wind energy research community, and in particular wind tunnel testing on such high-lift configurations have, to the best of the knowledge of the authors, not been published.

This work explores the challenges of the design and wind tunnel testing of a thick, multiple element, high-lift airfoil. A 40% thick flatback airfoil fitted with a leading edge slat of 30% of the main airfoil chord length was designed and subsequently tested in the LM Wind Power wind tunnel. The airfoil was designed using an optimizer coupled to the Navier-Stokes solver EllipSys2D, which proved to be a simple, robust and efficient design tool. A detailed parameter study exploring the dependence on the slat position and angle was carried out numerically and subsequently compared to experimental results for five slat positions. The paper will also discuss the challenges relating to wind tunnel testing of thick airfoils, in particular the 3D wall interference effects identified in the experiment.

In the following sections a summary is given of the methods used to design the airfoil and results from the numerical and experimental investigations are shown.

2 Multi-Element Airfoil Aerodynamics

To design an efficient multi-element airfoil it is necessary to have a basic understanding of how and why such a configuration can generate much higher lift coefficients compared to conventional single element airfoils. An explanation of the aerodynamic mechanisms responsible for generating high lift on multi-element airfoils can be found by consulting the extensive work by Smith [7]. Although this has also been explained in previous work by Gaunaa and Sørensen [1] it will for completeness be summarised in this work as well. Smith [7] outlines five main mechanisms at play:

1. **Slat effect:** Due to the circulation on the forward element (the slat), the pressure peak on the main element is reduced, which effectively delays the stall on the main element. An unavoidable consequence of this is that the load on the main element is reduced.
2. **Circulation effect:** Positioning the trailing edge of the forward element in the accelerated flow over the main element gives rise to an increase in the mean angle of the flow leaving the trailing edge of the forward element, increasing the circulation over this element.
3. **Dumping effect:** The accelerated flow at the trailing edge of the forward element makes it possible to 'dump' the forward element boundary layer at a much higher velocity than under free-stream conditions. This reduces the required pressure recovery, thus delaying stall and enabling high lift on the forward element.
4. **Off-the-surface pressure recovery:** Deceleration of the boundary layer from the forward element to free-stream velocity takes place in the wake of the forward element without contact with a wall, which is more efficient.
5. **Fresh boundary layer effect:** Breaking the flow into a number of independent boundary layers on each element helps delay separation since a thin and 'fresh' boundary layer is better capable of withstanding an adverse pressure gradient than a thick one.

The above conclusions can help narrowing down the design space when designing and positioning a slat relative to a main element. The forward element should thus be placed in close vicinity to the point of minimum pressure on the main airfoil to fulfil the first three items in the list. For thin airfoils this point would be quite far forward on the main element at approximately x/c=0.02, which is also reflected in the designs of slats for commercial aircraft. However, on a very thick airfoil this point is considerably further downstream at about x/c=0.1 to x/c=0.2. Lastly, item 5 above suggests that the boundary layers on the elements should not mix, suggesting some minimum distance between the elements exists below which the boundary layer profiles will mix and ruin the 'fresh boundary layer effect'.

The angle of the slat relative to the main airfoil as well as its shape depend on a number of factors that all interact. However, an optimal configuration in terms of maximum lift would be one where both elements stall at approximately the same (highest possible) angle of attack. Due to the upwash upstream of the main element the negative slat angle needs to be quite high to ensure that the flow does not stall prematurely on the slat.

3 2D Optimization of Multi-Element Airfoils

The optimization method developed for this work was programmed in Matlab, and uses the built-in optimization routine `fminsearch` which employs a simplex optimization method. This routine, however, is unbounded, and as such a community-developed wrapper routine named `fminsearchbnd` was used in combination with `fminsearch`, which allows for bounds on the optimization problem. The in-house flow solver EllipSys2D, see [4, 5, 8], was used for all CFD computations presented in this work. The grid generation procedure was fully automated using a combination of HypGrid2D [9] and Bash scripting, requiring only the geometry of the slat as input. The communication between Matlab and EllipSys2D was handled from a series of Bash scripts that exchanged input from files written by each code. Matlab ran in the background, outputting for each optimization step a file containing the coordinates of the slat as well as the required angle of attack. EllipSys was executed in parallel for maximum speed, and subsequently returned values of C_l and C_d for the given configuration. With a mesh of

19 blocks of 64^2 parallelized across 19 processors one CFD calculation completed in approximately 170 s yielding a total optimization time of 10 hours for 100 iterations (with two CFD calculations in each step) after which a converged result was typically obtained.

The overall goal of the optimization is to achieve a slat configuration which meets the target lift coefficients at an angle of attack which can be either specified or unspecified, while also providing a high maximum lift beyond the design point to provide enough lift reserve to tackle large changes in angle of attack.

The optimizer attempts to minimize a function which is composed of three factors: a penalty function which forces the optimizer towards achieving the desired lift coefficient, $C_{l,target}$, at the specified target angle of attack, α_{target}; the function A_1 which evaluates the lift-to-drag ratio at the target angle of attack; and finally the function A_2, which seeks to maximize the lift coefficient at some angle of attack, which the optimizer is free to tune. The two functions A_1 and A_2 are normalized with a predefined reference lift-to-drag ratio and lift coefficient.

$$CostFun = -Penalty\,(A_1 + A_2) \qquad (1)$$

with the $penalty$ function defined as

$$Penalty = exp\left(-\frac{(C_l(\alpha_{target}) - C_{l,target}))^2}{2\sigma_{penalty}}\right) \qquad (2)$$

where the penalty variance σ=0.02, and the two functions A_1 and A_2 is defined as

$$A_1 = \frac{C_l(\alpha_{target})}{C_d(\alpha_{target})} \cdot \frac{1}{(C_l/C_d)_{target,ref}} \cdot K_{optim} \qquad (3)$$

$$A_2 = \frac{C_l(\alpha)}{C_{l,maxref}} \cdot (1 - K_{optim}) \qquad (4)$$

K_{optim} is a factor in the range [0:1] which biases the cost function towards obtaining the target lift coefficient or lift-to-drag ratio. Although the lift-to-drag ratio is typically not as important towards the root section of a blade as it is further out on the blade, it is needed in this optimization method in order to force the optimization towards slat configurations where the flow is attached.

For each optimization iteration two evaluations are thus needed: one at the target angle of attack, and another at a free angle of attack which seeks to maximize C_l. Besides the angle of attack, the optimization code was allowed to vary the following geometrical parameters of the slat:

- Position of slat trailing edge measured as:
  - Surface distance along main airfoil surface from leading edge,
  - Normal distance from main airfoil surface to slat trailing edge.
- Slat angle relative to main airfoil.
- Slat camber (parabolic curve).

Figure 1 shows a schematic drawing of an airfoil fitted with a slat with the optimization parameters indicated.

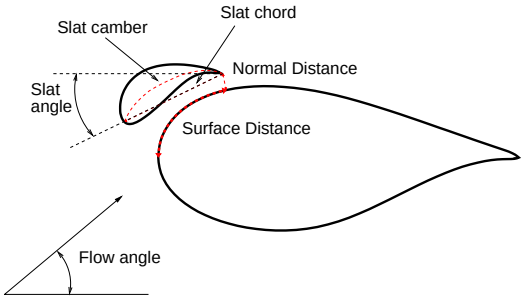

Figure 1: Geometrical parameters that the optimization code can adjust to meet the optimization targets.

The present study is based on the FFA-W3-360 airfoil which was modified in the following manner and used as main airfoil:

- Increased thickness from 36% chord to 40% chord,
- Opening of trailing edge from 3.24% chord to 5.39% chord.

The leading edge slat is also based on the FFA-W3-360 airfoil.

The parameter k_{optim} in the optimization algorithm (Eqns. 3, 4) controlled the weighing between emphasis on reaching the target lift or reaching the target lift-do-drag ratio, with k_{optim}=0 taking only the target lift into account and k_{optim}=1 only taking lift-to-drag into account. Four optimizations with different values of k_{optim} were carried out and it was found that k_{optim}=0.25 yielded the best result with both the highest maximum lift and relatively good lift-to-drag performance across a wide range of angles of attack.

Figure 2 shows the flatback airfoil fitted with the shape-optimized leading edge slat in it's

reference position. The optimization resulted in the slat being placed quite close to the surface at an angle and with a camber which created a distinct contraction between the main airfoil and the slat. The high angle of the slat is due to the significant upwash upstream of the airfoil configuration.

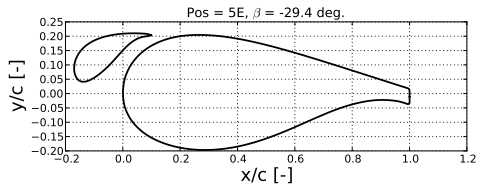

Figure 2: Optimized multiple element airfoil configuration .

Figure 3 shows a comparison of the chosen slat configuration with the baseline flatback 40% airfoil for both fully turbulent and transitional computations. As is evident, the lift of the slatted airfoil is not as sensitive to transition as the baseline airfoil, whereas both airfoils exhibit significant increases in the lift-to-drag ratio in the transitional computations. The small difference between the predicted lift for the fully turbulent and transitional computations indicate that this slatted airfoil could exhibit low sensitivity to surface roughness, which is a very desirable characteristic for wind turbine airfoils. The larger dependence seen in the lift-to-drag ratio is not as important on airfoil sections located near the root, since the drag component on the airfoil does not play a significant role close to the root.

4 Parameter Study

With the geometry of the slat fixed, a sensitivity study was carried out where a number of positions of the slat were investigated, allowing only the angle of the slat and the angle of attack to be optimized to reach the same goals as for the original optimization. These degrees of freedom corresponded to those in the wind tunnel tests where the slat position and angle were adjustable. A total of 42 positions were computed with 60 CFD computations for each slat position optimization.

Figure 4 shows contour plots of C_{l-max} and L/D_{max} for the 42 positions. Figure 5 show similar plots for an angle of attack 5 deg. lower than the optimized maximum lift angle of attack, which is more representative of the performance the slat would deliver under operational conditions. As is evident, high lift performance can be gained in a rather large but well-defined region around the position found by the optimization. The lift-to-drag ratio appears to have a maximum at the optimized position in Figure 4, which, however, for the lower angles of attack in Figure 5 is a more flat optimum. This corresponds well to the lift-to-drag ratios plotted in Figure 3, where the gradient in L/D generally is lower in ranges of angle of attack 8 deg. to 16 deg. than at angles close to stall.

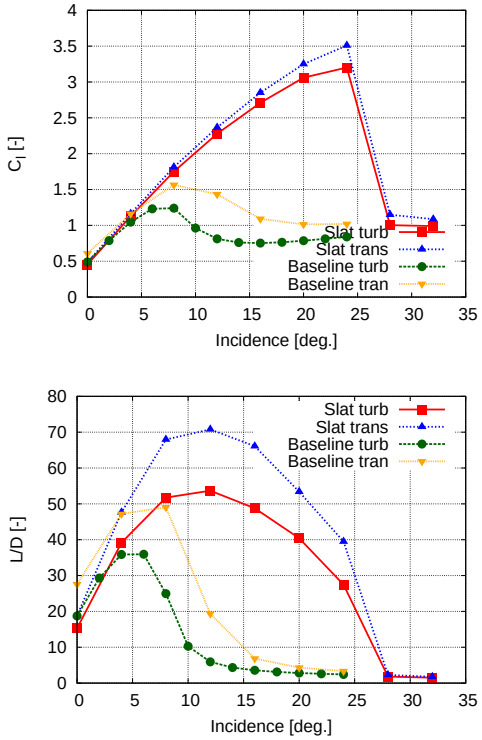

Figure 3: 2D lift coefficielt and lift to drag ratio as function of incidence for fully turbulent and transitional boundary layers (TI=0.1%).

5 Wind Tunnel Tests

Figure 6 shows the test setup for the airfoil fitted with a leading edge slat in a perspective view. The drawing shows the slat (in green) and the way in which it is mounted on the side wall (in purple). The main airfoil had a chord of 0.6 m and was fitted with 64 pressure taps, while the slat airfoil had a chord of 0.18 m and had 32 taps. By repositioning the slat leading

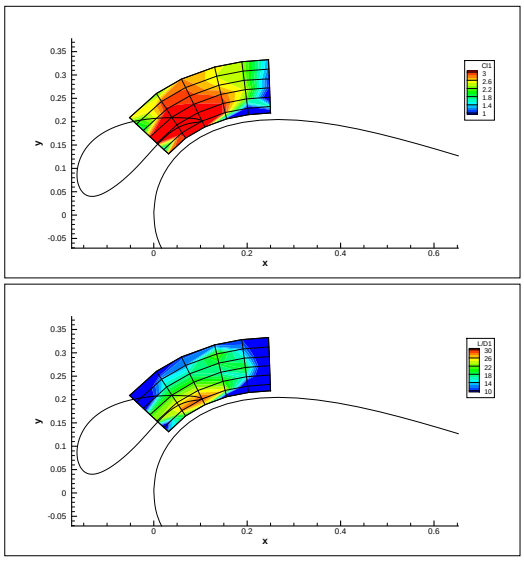

Figure 4: Parameter study of slat positioning showing contours of C_{l-max} and L/D at $\alpha_{C_{lmax}}$.

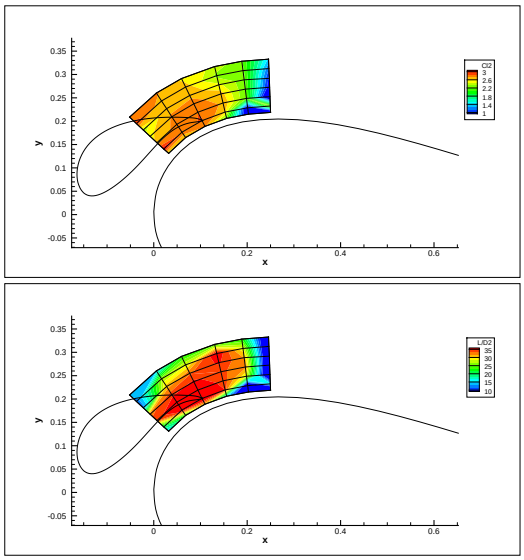

Figure 5: Parameter study of slat positioning showing contours of C_l and L/D at α=$\alpha_{C_{lmax}}$-5.

edge within the grid on the side wall and adjusting the stepless bracket (in dark red) the slat position and angle could be adjusted with a short turn-around time.

On the isolated flatback airfoil the following tests were performed:

- smooth surface, four Reynolds numbers: 1, 2, 3 and 4×10^6,
- Roughness, Vortex generators, Gurney flaps.

On the airfoil fitted with a slat the test matrix was more extensive since it involved repositioning of the slat:

- smooth surface, four Reynolds numbers: 1, 2, 3 and 4×10^6,
- Seven slat positions,
- Slat angle variations at five positions,
- Roughness, Vortex generators, Gurney flaps at one position.
- Flow visualization using wool tufts.

Since the wind tunnel tests served primarily towards validation of numerical methods, finding an optimal configuration of the slat configuration was not of priority. Based on the numerical parameter studies a number of slat positions were therefore chosen where the airfoil performance could be expected to vary relative to the reference position.

All wind tunnel tests presented in this work were carried out in the LM Wind Power Wind Tunnel. In this tunnel the lift is measured using either the surface pressure taps on the airfoil, the load cell, or the wall pressures. The drag is also measured three different ways: Using load cells, from integration of the surface pressures from the pressure taps on the airfoil, or using a wake rake. In this work all results that are shown are for the lift coefficient taken from the surface pressure and for the drag from the wake rake.

Figure 7 shows the lift and drag coefficients for the isolated flatback airfoil. At 5 degrees AOA the measured lift quite distinctly changes slope but the flow does not stall until an angle of attack of 13 degrees. This behaviour is not seen in the computations. Computations showed large dependence on turbulence intensity (TI) and based on the good agreement at low angle of attack a low TI of 0.2% was used in subsequent simulations both on the isolated and the slatted airfoil.

Figure 8 shows the lift and drag coefficients of the slat in the reference position '5E' showing lift coefficients of each airfoil element separately. The airfoil reaches a maximum lift coefficient just over 3 both in the computations and in the experiment, however, the computations predict stall considerably earlier than found in the experiment, which is in line with the results for the isolated flatback airfoil. Figure 9 shows the pressure distributions of the multi-element airfoil at 12 and 22 degrees angle of attack.

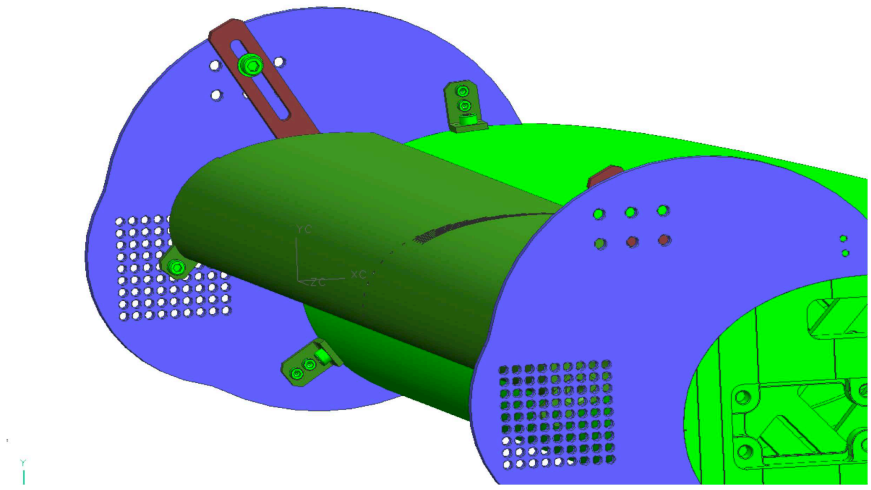

Figure 6: CAD drawing of the wind tunnel slat mounting designed by LM Wind Power.

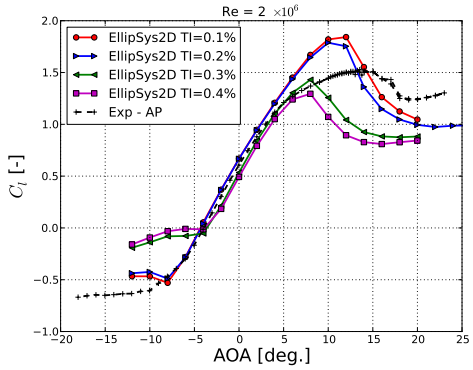

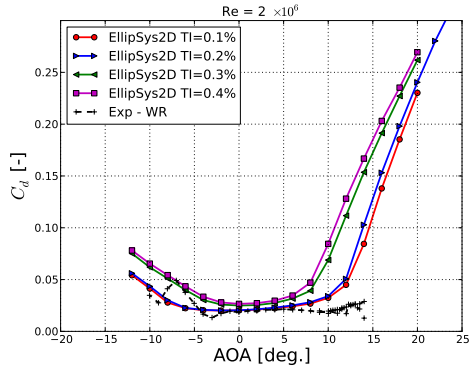

Figure 7: Lift and drag coefficients for the flatback airfoil at Re=2$\times 10^6$ computed with different inflow turbulence intensities.

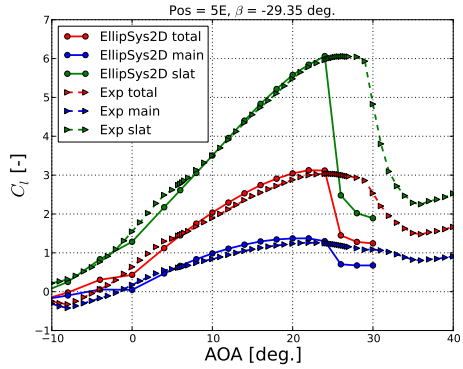

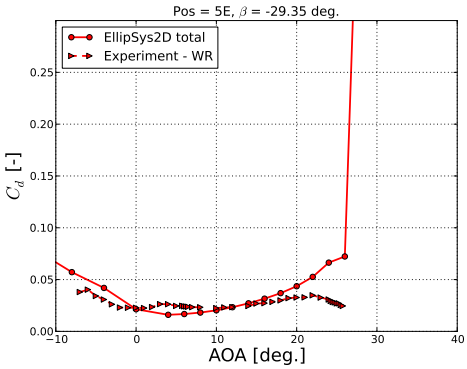

Figure 8: Lift and drag coefficients for the slatted airfoil with the slat in position 5E tested at Re=2$\times 10^6$. Note that the total lift is normalized with the main airfoil chord, while the lift coefficients for each element is normalized with their respective chord lengths.

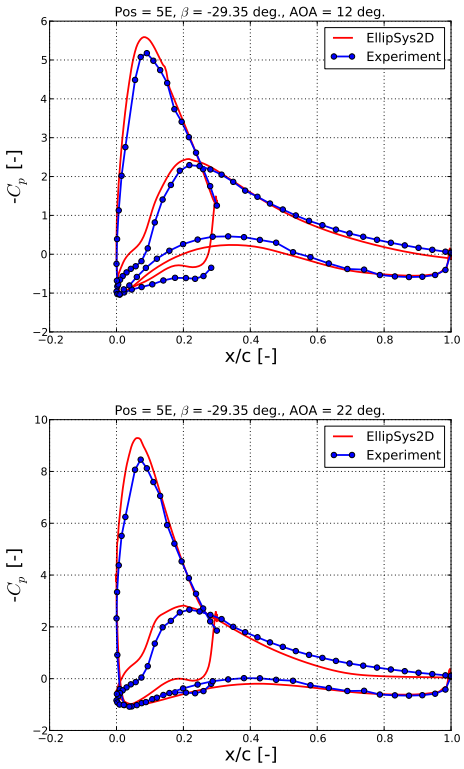

Figure 9: Pressure coefficients for the slatted airfoil with the slat in position 5E tested at Re=2$\times 10^6$. Note that the pressure distributions for both elements are plotted from x/c=0 although this is not their actual positions.

6 Wind Tunnel Effects

'2D' wind tunnel effects

To investigate to what degree the top and bottom wall of the wind tunnel had influence on the measurements, 2D CFD computations were carried out in a domain with top and bottom walls specified as symmetry conditions.

Figure 10 shows the lift and drag coefficients computed using a fully patched mesh which has no tunnel walls, and two overset grid simulations with and without tunnel walls compared to the wind tunnel measurement. Firstly, notice that there is a fairly large difference between the 'Std' fully pathced grid computations and the overset grid computations for angles of attack above 20 degrees with a significantly higher C_{l-max} in the overset simulations. Including the tunnel walls clearly has a significant influence on the lift coefficient, with an increase of 5% in C_{l-max}.

The computations with tunnel walls, are not, however, in better agreement with the measurements than the computations without walls. On the contrary, the discrepancy around C_{l-max} is even larger. However, at angles of attack below 5 degrees the measurements and tunnel grid simulations are in very good agreement.

Turning to the drag coefficient, including the tunnel appears to reduce the drag coefficient slightly, but not to the extent that the agreement with the experimental data becomes noticeably better.

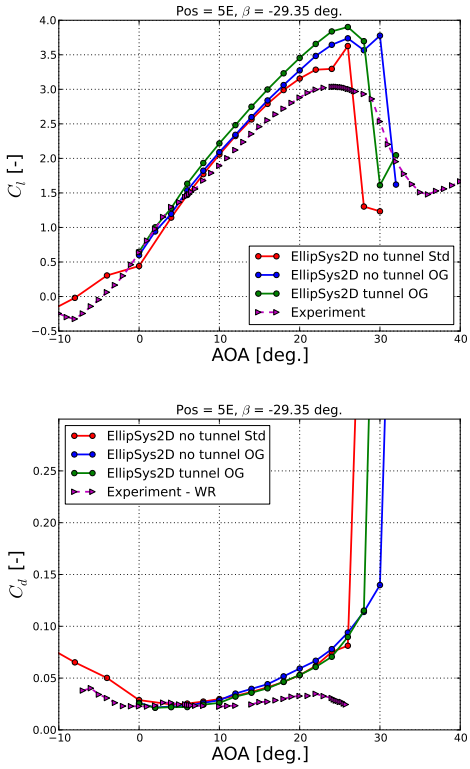

Figure 10: Lift and drag coefficients for the multi-element airfoil with the slat in position 5E tested at Re=2$\times 10^6$ in a 2D tunnel configuration.

3D flow effects due to wall interference

As evident from the results discussed, there were considerable discrepancies between the computations and wind tunnel measurements. Particularly the drag measurements were in very poor agreement with both the load cell drag and airfoil pressure drag increasing drastically for angles of attack over 5 degrees (not shown here). Something not observed in the wake rake measurements or in the 2D CFD simulations. The sudden increase in drag was accompanied by a change in slope of the lift

curve, something that was observed both for the isolated flatback airfoil and when fitted with the slat. It was hypothesised that this behaviour was caused by an onset of 3D flow caused by the side walls.

Flow visualizations were carried out using wool tufts mounted on the airfoil surfaces. These visualizations confirmed the hypothesis, which is clearly visible in Figure 12 which shows the airfoil operating at three different angles of attack. The picture is overlaid with lines highlighting the 3D flow structures showing two large flow structures emanating from the side walls, growing in extent with increasing angle of attack. To remedy this very undesirable flow feature it was attempted to mount vortex generators upstream of the point where the 3D flow structures occurred, both on the side walls and on the main airfoil. Although slight improvements were observed on the lift coefficient around the onset of its occurrence at 5 degrees angle of attack, no improvement was observed in the drag coefficient.

To further investigate to what extent the flow was three-dimensional over the airfoil surface, measurements were carried out where the wake rake was traversed laterally along the span of the airfoil model. Two angles of attack were investigated, with two measurements at each angle of attack. Figure 11 shows the drag coefficient as function of lateral position for 0 degrees and 15 degrees angle of attack. At 0 degrees angle of attack there is a fairly high variation along the span and also some difference between the two measurements suggesting that the flow may be unsteady even at low angles of attack. At 15 degrees angle of attack the drag also varies quite significantly along the span. At $\pm$ 250 mm spanwise position the Series 34 measurement measured a very high drag of 0.54, which is not seen to the same extent in Series 36. This suggests that the flow near the sides of the tunnel is highly unsteady.

The flow visualizations and wake rake traversals thus clearly demonstrated that the flow was not nominally 2D above 5 degrees angle of attack. The consequence of this was that flow measurements, whether sectional measurements as in the case of the airfoil pressure or integral as for the load cell, were fundamentally not 2D, making comparison of the experimental data to 2D CFD simulations very difficult. This finding supports the hypothesis that the change in lift curve slope at 5 degrees angle of attack was due to wall interference effects. As discussed by Rumsey et al. [6] it is very difficult to retain 2D flow characteristics near stall in wind tunnel measurements on high lift configurations. Side wall venting improved the flow quality considerable, but did not entirely remove the side wall effects. A continuation of the present work is under way, where side wall venting strategies will be investigated for thick, high lift airfoils. It it believed that side wall venting could also increase accuracy in stall for thinner airfoils.

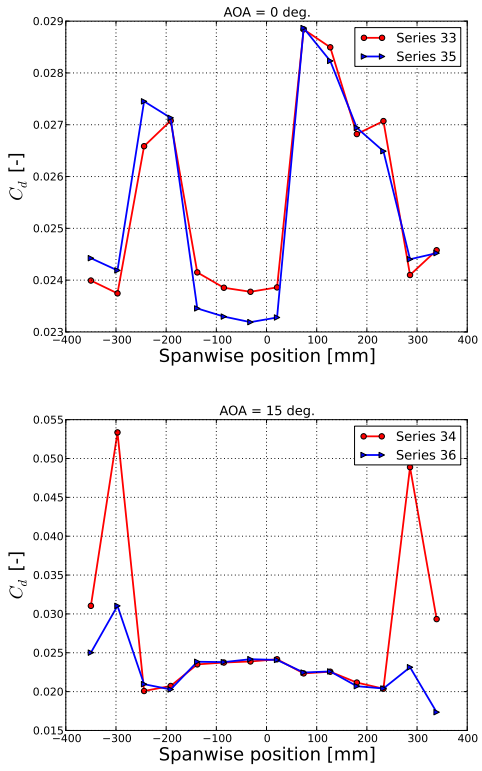

Figure 11: Drag coefficient as function of lateral measurement position for the multi-element airfoil with the slat in posiition 5E tested at Re=2$\times 10^6$. 0 mm is the center of the tunnel. The total tunnel width is 1400 mm.

7 Conclusions

Based on the results, a number of general tendencies observed in the measurements and computations were identified. Below, a summary is listed of the main conclusions of all the configurations investigated (which will all be presented in the final paper).

Summary of the main observations made from the experiment:

- The three sources of measurement for

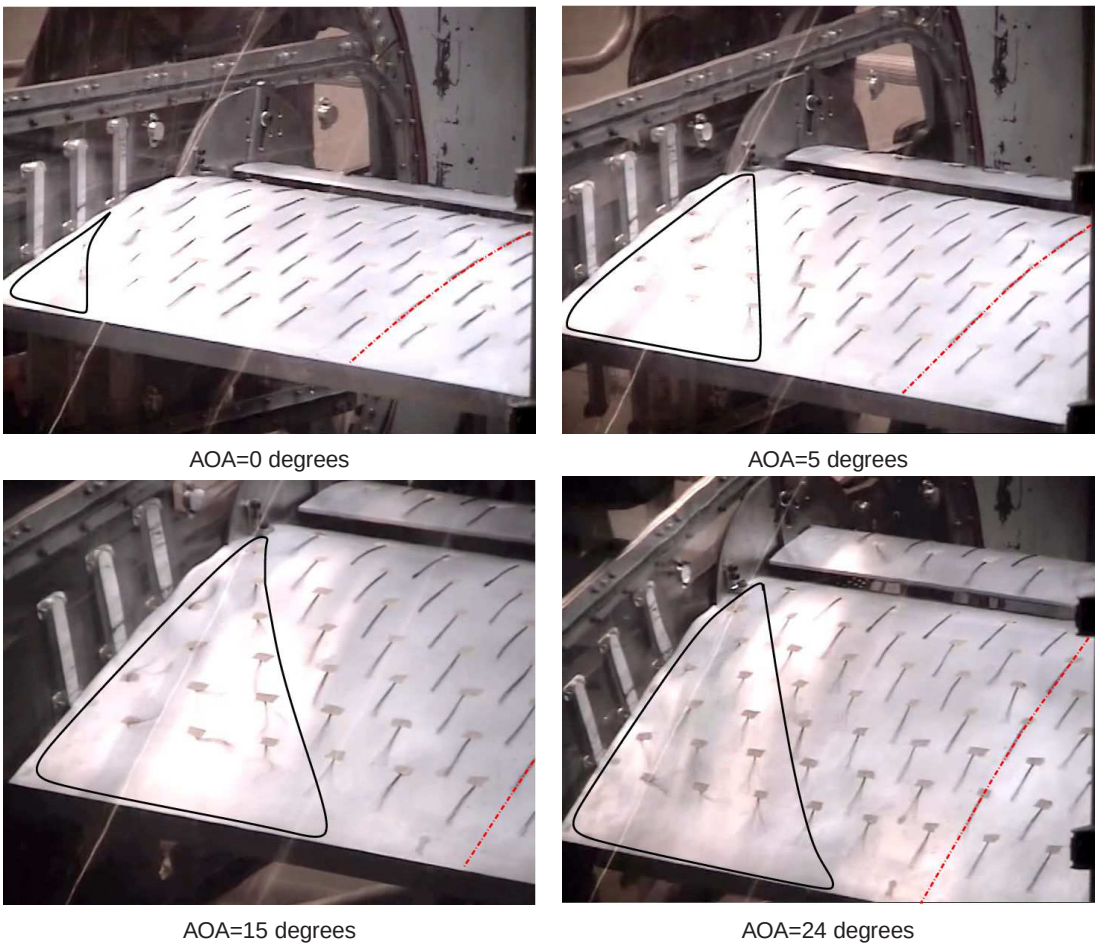

Figure 12: Wool tufts flow visualization of the slatted airfoil at various angles of attack.

both lift (Airfoil pressure, wall pressure, load cell) and drag (airfoil pressure, load cell, wake rake) were inconsistent above 5 degrees angle of attack, indicating the presence of 3D flow structures on the airfoil.

- The measurement data exhibited a 'kink' in the main element lift curve and subsequent change in slope around 5 degrees angle of attack for all configurations which was caused by the onset of 3D flow structures emanating from the side walls.
- The wake rake drag measurement was generally associated with uncertainty as well as inconsistency for some slat positions.

Summary of the main observations made in the CFD study:

- The computed lift on the slat airfoil was consistently in better agreement with the experiment than on the main airfoil.
- Trends due to changes in slat position and angle were to some degree predicted by CFD.
- The flow had a tendency to stall earlier on the main airfoil in the computations than in the experiment.
- The stall behaviour in the computations was generally more abrupt than in the experiment.
- For configurations where the two elements were in close proximity, the computations predicted higher suction in the gap region between the two elements.
- Including top and bottom walls in the 2D CFD simulations resulted in an increase in C_{l-max} of 5% with only little impact on the drag.

Acknowledgements

The work presented in the this paper has been carried out within the project "Aeroelastic Op-

timization of MW wind turbines" sponsored by the Danish Energy Council under contract EUDP-64009-0002. Wind tunnel measurements were carried out in collaboration with LM Wind Power. Computations were made possible by the use of the PC-cluster Gorm located at the Risø-DTU central computing facility.

References

[1] M. Gaunaa and N. N. Sørensen. Thick multiple element airfoils for use on the inner part of wind turbine rotors. In *The Science of Making Torque from Wind*, Crete, Greece, June 2010.

[2] J. Johansen, H. A. Madsen, M. Gaunaa, and B. Christian. Design of a wind turbine rotor for maximum aerodynamic efficiency. *Wind Energy*, 12:261–273, 2009.

[3] H. A. Madsen. Two modifications of the BEM method based on validation with results of actuator disc results. Technical Report Risø-R-1611(EN), Risø National Laboratory for Sustainable Energy DTU, 2006.

[4] J. A. Michelsen. Basis3D—a platform for development of multiblock PDE solvers. Technical Report AFM 92-05, Technical University of Denmark, 1992.

[5] J. A. Michelsen. Block structured multigrid solution of 2D and 3D elliptic PDEs. Technical Report AFM 94-06, Technical University of Denmark, 1994.

[6] C. L. Rumsey, E. M. Lee-rausch, and R. D. Watson. Three-dimensional effects in multi-element high lift computations. *Computers & Fluids*, 32:631–657, 2003.

[7] A. M. O. Smith. High-Lift Aerodynamics. *Journal of Aircraft*, 12(6):501–530, June 1975. ISSN 0021-8669. doi: $10.2514/3.59830$.

[8] N. N. Sørensen. General purpose flow solver applied to flow over hills. Technical Report Risø-R-827(EN), Risoe National Laboratory, 1995.

[9] N. N. Sørensen. HypGrid2D—a 2-D mesh generator. Technical report, Risø-R-1035(EN), Risoe National Laboratory, 1998.

[10] N. N. Sørensen. Prediction of multi-element airfoils with the EllipSys code. In T. Buhl, editor, *Research in Aeroelasticity EFP-2007-II*, number Risø-R-1698(EN), chapter 3. 2007.